EARTH SURFACE PROCESSES AND LANDFORMS
Earth Surf. Process. Landforms **41**, 2111–2122 (2016)
Copyright © 2016 John Wiley & Sons, Ltd.
Published online 10 July 2016 in Wiley Online Library
(wileyonlinelibrary.com) DOI: 10.1002/esp.3977

Characterizing supraglacial meltwater channel hydraulics on the Greenland Ice Sheet from *in situ* observations

Colin J. Gleason,[1]* Laurence C. Smith,[2] Vena W. Chu,[3] Carl J. Legleiter,[4,5] Lincoln H. Pitcher,[2] Brandon T. Overstreet,[5] Asa K. Rennermalm,[6] Richard R. Forster[7] and Kang Yang[2]
[1] Department of Civil and Environmental Engineering, University of Massachusetts, Amherst, MA, USA
[2] Department of Geography, University of California, Los Angeles, CA, USA
[3] Department of Geography, University of California, Berkeley, CA, USA
[4] Geomorphology and Sediment Transport Laboratory, US Geological Survey, Golden, CO, USA
[5] Department of Geography, University of Wyoming, Laramie, WY, USA
[6] Department of Geography, Rutgers, The State University of New Jersey, New Brunswick, NJ, USA
[7] Department of Geography, University of Utah, Salt Lake City, UT, USA

Received 21 December 2015; Revised 9 May 2016; Revised 2 May 2016; Accepted 10 May 2016

*Correspondence to: Colin J Gleason, Department of Civil and Environmental Engineering, University of Massachusetts, Amherst, MA, USA. E-mail: cjgleason@umass.edu

ESPL
Earth Surface Processes and Landforms

ABSTRACT: Supraglacial rivers on the Greenland Ice Sheet (GrIS) transport large volumes of surface meltwater toward the ocean, yet have received relatively little direct research. This study presents field observations of channel width, depth, velocity, and water surface slope for nine supraglacial channels on the south-western GrIS collected between July 23 and August 20, 2012. Field sites are located up to 74 km inland and span 494–1485 m elevation, and contain measured discharges larger than any previous *in situ* study: from 0.006 to 23.12 m^3/s in channels 0.20 to 20.62 m wide. All channels were deeply incised with near vertical banks, and hydraulic geometry results indicate that supraglacial channels primarily accommodate greater discharges by increasing velocity. Smaller streams had steeper water surface slopes (0.74–8.83%) than typical in terrestrial settings, yielding correspondingly high velocities (0.40–2.60 m/s) and Froude numbers (0.45–3.11) with supercritical flow observed in 54% of measurements. Derived Manning's *n* values were larger and more variable than anticipated from channels of uniform substrate, ranging from 0.009 to 0.154 with a mean value of 0.035 ± 0.027 despite the absence of sediment, debris, or other roughness elements. Ubiquitous micro-depressions in shallow sections of the channel bed may explain some of these roughness values. However, we find that other, unobserved sources of flow resistance likely contributed to these elevated Manning's *n* values: future work should explicitly consider additional sources of flow resistance beyond bed roughness in supraglacial channels. We conclude that hydraulic modeling for these channels must allow for both subcritical and supercritical flow, and most importantly must refrain from assuming that all ice-substrate channels exhibit similar hydraulic behavior, especially for Froude numbers and Manning's *n*. Finally, this study highlights that further theoretical and empirical work on supraglacial channel hydraulics is necessary before broad scale understanding of ice sheet hydrology can be achieved. Copyright © 2016 John Wiley & Sons, Ltd.

KEYWORDS: Greenland; supraglacial rivers; supraglacial streams; channel hydraulics; climate change

Introduction

Recent decades have seen a surge in scientific interest in glaciers and ice sheets as climate change dramatically alters their role in the global climate system. In particular, the Greenland Ice Sheet (GrIS) has attracted widespread study as a vast store of freshwater that could be released into the ocean, leading to increasing rates of global sea level rise and changes in ocean circulation patterns. Numerous studies have estimated the freshwater runoff from the GrIS using a combination of gravimetry and/or climatological and glaciological modeling (e.g. Zwally *et al.*, 2005; Rignot *et al.*, 2008; van den Broeke et al., 2009; Schrama *et al.*, 2011; Zwally *et al.*, 2011; Sasgen *et al.*, 2012; Barletta *et al.*, 2013; Andersen *et al.*, 2015), whereas fewer studies have attempted to use pro-glacial river discharge to directly estimate runoff to the ocean (Mernild and Hasholt, 2009; Mikkelsen *et al.*, 2013; Hasholt *et al.*, 2013; Rennermalm *et al.*, 2013a; Fitzpatrick *et al.*, 2014, Lindbäck *et al.*, 2015; Overeem *et al.*, 2015; Smith *et al.*, 2015). This body of work has revealed that outflow of liquid water accounts for at least half of the mass loss from the GrIS (van den Broeke *et al.*, 2009; Enderlin, 2014), and this meltwater is generated on the surface of the ice sheet and creates a complex and perennial network of supraglacial streams, rivers, and lakes (Nobles, 1960; Ferguson, 1973; Rennermalm *et al.*, 2013b; Chu, 2014). Supraglacial rivers in particular play an important role in transporting large volumes of meltwater across the ice surface and into moulins, vertical conduits that transport surface

water to the sub-glacial system and out to the ocean (Smith *et al.*, 2015). Despite emerging understanding of the importance of these channels, supraglacial rivers are understudied and basic supraglacial fluvial science remains in an early stage of development.

Supraglacial rivers and streams received relatively little scientific attention between the 1980s and quite recently, and the current surge in interest is attributed mostly to increased use of remotely sensed data. For instance, Joughin *et al.* (2013) used high-resolution imagery (2 m) to manually delineate streams in a small area in western Greenland, showing a trellis drainage pattern where streams flow transverse to the direction of ice flow. Lampkin and Vanderberg (2014) tracked large channels using Landsat imagery (30 m) throughout a melt season and found that the total number of channels and the mean length of active channels increases during the melt season, with higher-order networks only developing above 800 m elevation above mean sea level. Poinar *et al.* (2015) similarly found that rivers tend to lengthen at higher elevations (finding ~6 km streams at 1200 m elevation compared to ~40 km streams at 1700 m elevation). Smith *et al.* (2015) used automated extraction of stream networks (following Yang and Smith, 2013) to characterize the supraglacial hydrology for a region of south-western Greenland, and found well-developed river networks dominated by the presence of moulins at elevations up to ~1600 m. Legleiter *et al.* (2014) demonstrated that water depth in these supraglacial streams could be inferred from high-resolution (2 m) multispectral satellite images. Finally, Yang *et al.* (2015) showed that GrIS supraglacial river networks do not conform to expectations based on GrIS surface digital elevation models (DEMs) and traditional terrestrial watershed delineation techniques, and Yang *et al.* (2016) characterized the morphometry of these networks.

These more recent remote sensing studies have mapped hundreds of larger channels at a broad spatial scale, but have revealed little about their local hydraulics. This knowledge gap in turn limits current understanding of supraglacial channels in the context of terrestrial fluvial hydrology and hydraulic theory, and highlights the need for fieldwork to inform remote sensing studies. A small field-based scientific literature that considers the hydraulics of supraglacial channels does exist, with most studies conducted before the late 1980s. Early research focused on small (discharge less than 1 m^3/s) streams near the margins of temperate alpine glaciers. Following Ferguson's (1973) discovery of the perennial nature of these marginal streams, other researchers were interested in their hydraulic geometry, meandering behavior, and longitudinal profile (Knighton, 1972, 1981, 1985; Parker, 1975; Marston, 1983). More recently, McGrath *et al.* (2011) published a detailed field study of one supraglacial stream catchment in western Greenland, recording a stream incision rate of 3.3 $\pm$ 0.47 cm/day and a discharge of 0.17 $\pm$ 0.04 m^3/s at the outlet of the catchment ~6 km from the ice edge. They noted that stream discharge only accounted for 52% of catchment meltwater production, with crevasses capturing the remaining runoff. None of these previous field studies occurred on the interior of ice sheets or glaciers, where crevassing is rare. In addition, most of the streams examined were on a scale too small to be observed in even high resolution satellite imagery, with channels often less than 40 cm wide.

More recently, researchers have sought deeper understanding of supraglacial hydraulics through creation of theoretical models of channel evolution (e.g. Jarosch and Gudmundsson, 2012; Karlstrom *et al.*, 2013; Kingslake and Sole, 2015; Karlstrom and Yang, 2016). Using these models, both Jarosch and Gudmundsson (2012) and Karlstrom *et al.* (2013) found that the relationship between channel incision rate and overall ice sheet ablation rate exerts strong controls on the resulting planform morphology of supraglacial streams. These recent studies also highlight the marked differences between supraglacial and terrestrial streams: little to no sediment transport on the GrIS and strong thermal control renders many theories of terrestrial channel evolution and morphological change irrelevant. To date, no detailed field study has been made for streams/rivers of the interior GrIS, and a compelling need therefore exists for basic, field-based studies of supraglacial channels to develop fluvial science on the GrIS.

In this paper, we characterize the hydraulics of nine different supraglacial channel reaches atop the GrIS, ranging from the ice edge (494 m elevation) to 74 km inland (1485 m elevation). These sites include rivers two orders of magnitude larger than any previously studied *in situ*, allowing for comparison with larger terrestrial streams and more directly informing remote sensing studies of the ice sheet surface. We analyze the basic hydraulics of these channels, both at-a-station and in a downstream direction, and compare our findings with those previously made for smaller scale alpine supraglacial environments and with terrestrial systems found on similar scales. We conclude with a synthesis of our findings and previous literature in an effort to guide future modeling and remote sensing studies of supraglacial channels.

Data and methods

All data used in this study were collected in July and August of 2012, shortly after one of the most extreme surface melt events in the modern history of the GrIS (Hall *et al.*, 2013; Tedesco *et al.*, 2013). Data were collected in a transect from 494 to 1485 m elevation, yielding nine separate datasets from six separate locations used to assess supraglacial hydraulics (Figure 1). These locations are all contained within the hydrologic potential basin of the Isortoq River and Issunguata Sermia glacier (as delineated by Lindbäck *et al.*, 2015). Five of these datasets were collected in a downstream direction over reach lengths of 55 to 1093 m, whereas four datasets were collected at-a-station over a period of less than two hours. Taken collectively, these nine datasets span a wide range of stream and river scales (0.20–20.62 m width) and an elevational transect across much of the ablation zone. Table I gives positions and dates for each measurement in this study.

We adopted a channel naming convention after a combination of data collection type (at-a-station or downstream) and elevation; for example, AAS1328 is at-a-station data with elevation of 1328 m, and DS904 is downstream data with a highest reach elevation of 904 m. In addition to this convention, there are three channels with extra nomenclature. One reach has data of both types (AAS1485 and DS1485), one channel has downstream data collected on two separate days at adjacent reaches (DS534 upper and DS534 lower), and one channel has at-a-station data at two different cross-sections (AAS1196 upper and AAS1196 lower).

Field measurements of channel elevation, width, cross-sectional depth, velocity, and water surface slope were collected in one of two ways: using manual channel-survey techniques in small streams, or using a Sontek River Surveyor S5 acoustic Doppler current profiler (ADCP) in larger channels. Manual channel-survey techniques were applied for four reaches: DS904, DS534 upper, DS534 lower, and DS502, and their elevations were recorded with a Garmin eTrex handheld global positioning system (GPS) unit. For these channels, measurements were taken at 6 to 19 cross-sections orthogonal to thalweg flow direction. Width was measured by laying a stadia rod across the stream. Depth was measured in equally

Copyright © 2016 John Wiley & Sons, Ltd.

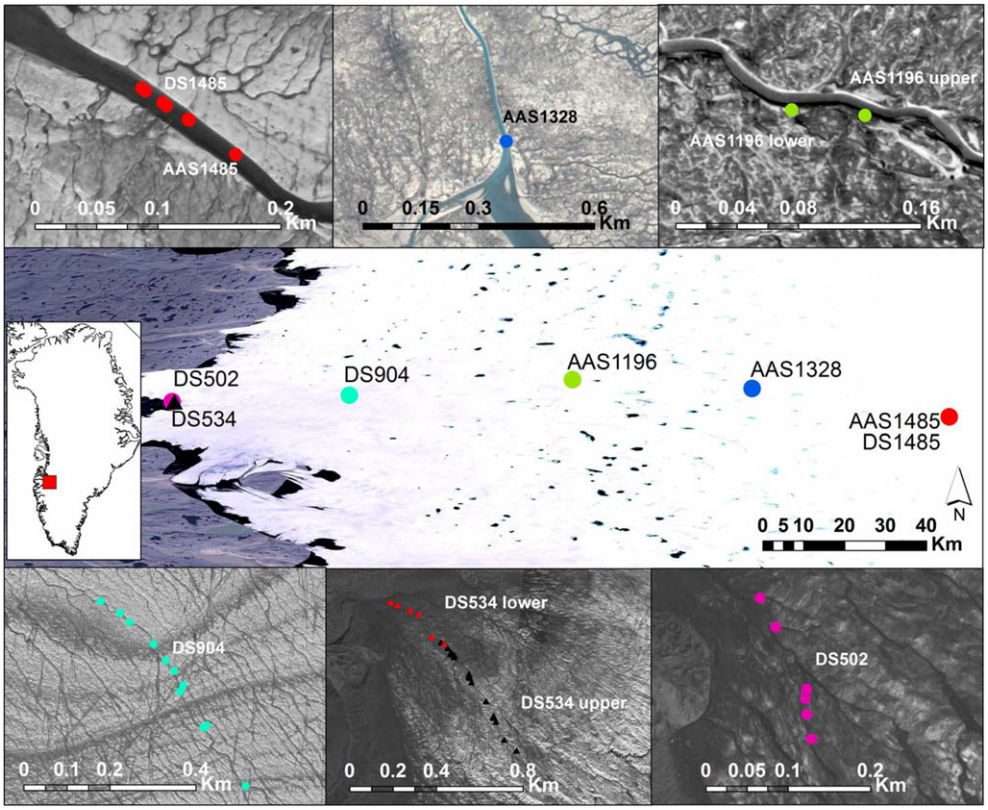

Figure 1. Nine hydraulic datasets were collected from six different locations on the Greenland Ice Sheet (GrIS). Field sites are located from 494 to 1485 m elevation and from the ice edge up to 74 km inland. All sites are contained within the hydrologic potential basin of the Issunguata Sermia glacier, and span nearly the entire ablation zone. Discharges in the larger rivers at higher elevation (sites AAS1196, AAS1485, AAS1328, and DS1485) were measured by an acoustic Doppler current profiler (ADCP) while the lower elevation sites (DS904, DS534, DS502) were measured on foot using manual field techniques. This figure is available in colour online at wileyonlinelibrary.com/journal/esp

spaced intervals by inserting a metric rod orthogonal to the stadia rod extending to the channel bed, and then averaged to yield an average depth (d). Surveying the channels in this manner also allowed for calculation of hydraulic radius (R), and in cases where the stream was too deep to enter safely, a ladder was used as a span from which to collect measurements (Figures 2c and 2d). Stream surface velocity was measured by using a FloWav Phaser V1000 portable Doppler radar velocity meter to measure surface velocity, collected over a one-minute interval. We were not able to measure velocity within the water column at most cross-sections due to both safety considerations and the fact some streams were too shallow to insert instruments available to us at depth. Finally, water surface slope was measured via optical survey using a CST/ Berger 32X autolevel and stadia rod, and upstream and downstream points for calculating slope at each cross-section were located approximately 20 channel widths apart. All of these field measurements were made by walking upstream, and span reaches ranging from 55 to 1093 m. Measurements in the sites labeled as DS were all collected within three hours of the first measurement in each dataset.

For the other five study reaches (AAS1196 upper, AAS1196 lower, AAS1485, AAS1328, and DS1485), the ADCP was used to collect depth and velocity data. The ADCP was deployed from a specially designed riverboard secured to a portable cableway extended across the channel with helicopter support (Figures 2a and 2b). The ADCP collected cross-stream and streamwise vertical velocity for a number of discrete cells distributed vertically throughout the water column; an integrated real time kinematic (RTK) GPS recorded ADCP positions with a precision of ±0.03 m in both the vertical and horizontal directions. Despite the exceptional water clarity of these supraglacial rivers (and thus low number of acoustic reflectors), the ADCP maintained acceptable signal/noise ratios within the range specified by the manufacturer. A cross-sectional mean velocity was calculated by taking the average of all of the vertical cells for a given location in the cross-section and then calculating the mean of these depth-averaged velocities across the channel. The onboard RTK GPS was also used to determine river width and water surface slope. Width was calculated directly from the GPS position measurements, and slope was obtained by establishing two ADCP transects in close proximity to one another and using the difference in elevation between the two sites to calculate slope (Figure 1). While GPS measurements often have limited accuracy and precision in the vertical dimension, the use of RTK corrections from a local base station provided much greater positional precision and therefore more accurate slopes and widths. River depth measurements were taken continuously by the ADCP while traversing the channel, and a cross-sectional mean depth was calculated by averaging all depths across the transect. For each measurement, the ADCP made two consecutive passes (e.g. first starting stream left and then starting stream right, from the perspective of looking downstream), and an in-the-field quality check was made to ensure that the discharges recorded on each pass matched one another to within 5%. Finally, the ADCP was floated downstream for 159 m at site AAS1485 to establish a longitudinal water surface profile.

Measurements of width, depth, velocity, and slope were made in the field, and used to calculate the following derived hydraulic quantities: river discharge (Q) as the product of cross-sectional area and average velocity, Froude number (Fr, Equation 1), Manning's n (Equation 2), stream power (Ω, Equation 3), and both at-a-station (AHG) and downstream (DHG) hydraulic geometry (Leopold and Maddock, 1953; Equations 4–6) for each study reach. Please refer to Table II for a summary of this nomenclature. Average velocity was used

Copyright © 2016 John Wiley & Sons, Ltd.

Table I. Locations and dates of each measurement in this study

Latitude	Longitude	Elevation (m)	Date	Site
67.16558	−49.64615	879	July 23, 2012	DS904
67.16517	−49.64572	881	July 23, 2012	
67.16447	−49.64433	885	July 23, 2012	
67.16333	−49.64183	887	July 23, 2012	
67.16282	−49.63997	889	July 23, 2012	
67.16237	−49.63918	890	July 23, 2012	
67.16208	−49.63857	893	July 23, 2012	
67.16153	−49.63683	896	July 23, 2012	
67.16072	−49.63505	898	July 23, 2012	
67.15800	−49.63098	904	July 23, 2012	
67.15296	−50.03984	494	August 20, 2012	DS502
67.15266	−50.03934	500	August 20, 2012	
67.15202	−50.03833	500	August 20, 2012	
67.15192	−50.03834	500	August 20, 2012	
67.15175	−50.03827	502	August 20, 2012	
67.15149	−50.03808	500	August 20, 2012	
67.15252	−50.03502	511	August 9, 2012	DS534 upper
67.15235	−50.03465	499	August 9, 2012	
67.15215	−50.03418	504	August 9, 2012	
67.15212	−50.03428	505	August 9, 2012	
67.15212	−50.03410	504	August 9, 2012	
67.15200	−50.03387	500	August 9, 2012	
67.15207	−50.03385	503	August 9, 2012	
67.15135	−50.03215	506	August 9, 2012	
67.15125	−50.03213	505	August 9, 2012	
67.15120	−50.03203	505	August 9, 2012	
67.15102	−50.03180	507	August 9, 2012	
67.15030	−50.03010	520	August 9, 2012	
67.14967	−50.02918	518	August 9, 2012	
67.14972	−50.02917	519	August 9, 2012	
67.14965	−50.02910	518	August 9, 2012	
67.14950	−50.02887	521	August 9, 2012	
67.14878	−50.02782	530	August 9, 2012	
67.14838	−50.02640	534	August 9, 2012	
67.15255	−50.03537	503	August 9, 2012	
67.15401	−50.04110	496	August 15, 2012	DS534 lower
67.15392	−50.04032	498	August 15, 2012	
67.15374	−50.03893	500	August 15, 2012	
67.15363	−50.03800	500	August 15, 2012	
67.15275	−50.03643	506	August 15, 2012	
67.15250	−50.03503	508	August 15, 2012	
67.11954	−48.33133	1485	July 20, 2012	DS1485
67.11952	−48.33126	1485	July 20, 2012	
67.11943	−48.33085	1485	July 20, 2012	
67.11945	−48.33092	1486	July 20, 2012	
67.11934	−48.33043	1485	July 20, 2012	
67.11933	−48.33041	1485	July 20, 2012	
67.20100	−49.15840	1197	July 23, 2012	AAS1196 upper
67.20100	−49.15950	1197	July 23, 2012	AAS1196 lower
67.18160	−48.76490	1327	July 23, 2012	AAS1328
67.11910	−48.32951	1449	July 20, 2012	AAS1485

Note: The datum for these data is WGS84, and the coordinates are unprojected.

to calculate these quantities for the larger ADCP-measured rivers, whereas the measured surface velocity was used in the case of the smaller streams. These differing velocities were used to ensure the fidelity of derived quantities to *in situ* measurements, and the following section shows the impact of this decision on the quantities derived from Equations 1–6:

$$\mathrm{Fr} = \frac{v}{\sqrt{gd}} \tag{1}$$

$$n = \frac{1}{v} R^{2/3} S^{1/2} \tag{2}$$

$$\Omega = \rho g Q S \tag{3}$$

$$w = aQ^b \tag{4}$$

$$d = cQ^f \tag{5}$$

$$v = kQ^m \tag{6}$$

These derived hydraulic variables allow for comparison of our field data with data published for both smaller supraglacial streams and for terrestrial rivers. DHG is traditionally calculated by using a Q of fixed frequency (e.g. mean annual flow in the original work by Leopold and Maddock, 1953; bankfull flow more recently, Gleason, 2015). Here, we assume that our downstream field measurements were made at a constant forcing discharge that constitutes such a fixed frequency for the day and time period over which they were collected.

Sensitivity of derived hydraulics to velocity

The velocity-dependent derived hydraulic quantities (Q, Fr, n) were calculated from two different measures of velocity: average velocity in the case of ADCP measurements and surface velocity in the case of traditional field techniques. Thus, n and Fr are not directly comparable across our two measurement scales, and we here calculate surface velocity from average velocity (and vice versa) in a sensitivity analysis to determine the effect of using different measured velocities on our results.

In terrestrial open-water channels, velocity typically increases as a function of distance from the bed as the effect of frictional resistance from the bed diminishes over the first 50–90% of the flow depth toward the free surface at the top of the water column. While this vertical velocity profile is the subject of much research, one simple approximation invokes a power law given by:

$$v = pd^x \tag{7}$$

Furthermore, if Manning's equation is assumed to hold, then $x = 1/6$ (Mueller, 2013). The surface velocity is equal to the value of Equation 7 when $d = d_{max}$, where d_{max} is the total flow depth, and thus the coefficient p is given by Equation 8:

$$p = \frac{v_{surf}}{d_{max}^{1/6}} \tag{8}$$

The average velocity ($\overline{v}$) of such a profile is then equivalent to Equation 9,

$$\overline{v} = \frac{\int_0^{d_{max}} p d^{1/6} dd}{d_{max}} \tag{9}$$

which may be solved, combined with Equation 8, and simplified to yield Equation 10.

$$\overline{v} = \frac{v_{surf}}{x+1} \tag{10}$$

Copyright © 2016 John Wiley & Sons, Ltd.

Figure 2. Field measurements were made in two ways: using an acoustic Doppler current profiler (ADCP) (a–b), and using traditional field methods (c–d). Helicopter support was leveraged to deploy the ADCP on rivers larger than ever before studied *in situ*, whereas manual field investigation allowed for numerous detailed measurements over a five-day ice camp. These field methodologies ultimately yielded data on streams of two different scales, allowing us to compare channels across these scales and allowing comparison with a wider range of terrestrial and previously studied supraglacial systems. This figure is available in colour online at wileyonlinelibrary.com/journal/esp

Thus, given $x = 1/6$, the average velocity is always equal to ~85% of the surface velocity. Alternatively, standard approximations based on a logarithmic velocity profile described by the law of the wall imply that the average velocity is found at $0.6 \times d$ (Robert, 2003). Substituting this depth–velocity pair yields Equation 11,

$$\overline{v} = v_{surf} 0.6^{1/6} \tag{11}$$

which implies that the depth-averaged velocity is ~92% of the surface velocity. While both of these cases make strict assumptions of a power law velocity profile with an exponent of 1/6, they agree with Rantz *et al.*'s (1982) empirical conclusions that average velocity is smaller than surface velocity by a factor 0.85 or 0.86 for a natural channel and by a factor of 0.90 for a smooth artificial channel. Therefore, we assess the sensitivity of our derived hydraulic variables using Equation 10, which agrees with Rantz *et al.* (1982) and represents the maximum expected difference between surface and depth-averaged velocities.

Results

Our field efforts provided data from supraglacial melt channels of two distinct scales: smaller streams with discharges between 0.006 and 0.402 m^3/s collected on foot using manual field methods, and larger rivers with discharges between 4.58 and

Table II. Nomenclature

Symbol	Unit	Measured/derived	Description
w	m	Measured	Width
d	m	Measured	Depth
$\overline{v}$	m/s	Measured	Average velocity (average in a vertical profile for a given station)
v_{surf}	m/s	Measured	Surface velocity
S	m/m	Measured	Channel slope
g	m/s^2	Constant	Acceleration due to gravity
Fr	–	Derived	Froude number (indicator of critical flow)
n	–	Derived	Manning's roughness coefficient (a friction factor)
Ω	N/s	Derived	Stream power (energy dissipation per unit length)
Q	m^3/s	Derived	Discharge (volumetric flow rate)
AHG			At-a-station hydraulic geometry
DHG			Downstream hydraulic geometry
a	–	Derived	Width hydraulic geometry coefficient (scale parameter)
b	–	Derived	Width hydraulic geometry exponent (sensitivity of Q to w)
c	–	Derived	Depth hydraulic geometry coefficient (scale parameter)
f	–	Derived	Depth hydraulic geometry exponent (sensitivity of Q to d)
k	–	Derived	Velocity hydraulic geometry coefficient (scale parameter)
m	–	Derived	Velocity hydraulic geometry exponent (sensitivity of Q to v)

Copyright © 2016 John Wiley & Sons, Ltd.

23.12 m^3/s collected via ADCP (Figures 3 and 4). The observed velocities at both scales were similar, ranging from 0.40 to 2.60 m/s. The larger, ADCP measured rivers were wider and deeper, with a width range of 7.19 to 20.62 m compared to 0.20 to 3.84 m and a depth range of 0.47 to 2.21 m compared to 0.03 to 0.40 m (Figures 3, 4, Table III). Width/depth ratios were generally higher and more variable in the smaller streams (ranging from 1.2 to 42.2) than in the larger rivers (ranging from 6.8 to 17.3). Width/depth ratios for the larger channels are similar to those found by Knighton (1985) in streams with discharge less than 0.052 m^3/s, where Knighton's width/depth ratios ranged from 3.4 to 12.

All channels were free of debris (i.e. wood and sediment) and visually observed to be almost entirely devoid of suspended sediment. Channels at both scales exhibited cryoconite pitting on the channel bed (see Figure 2c and cryoconite holes in Figure 2d). Cryoconite forms when airborne sediment settles in micro depressions in the ice sheet surface, thus raising local albedo and leading to faster melting than the surrounding ice to create 'cryoconite holes' on the surface (MacDonell and Fitzsimons, 2008; Boggild *et al.*, 2010; Wientjes *et al.*, 2011; Tedesco, 2013). Cryoconite was present in depressions on the channel bed at nearly every measurement site for the smaller scale streams in our study, but was not present in any of the larger rivers, despite widespread cryoconite deposits adjacent to the channel in the latter sites.

Our field investigation documented a wide range and large maximum values of slope across streams of both scales, and thus highly variable velocity and Fr. The larger rivers in this study had low slopes ranging from 0.01 to 0.36%, which in turn led to Fr ranging between 0.07 and 0.80 (Figure 3). These low slopes were a product of site selection, as safety concerns limited our cableway setup to these gentler sections. Both slope and Fr lacked central tendency, with coefficients of variation of 0.76 and 0.92, respectively. The maximum Fr of 0.80 indicates that these low slope rivers were always measured under subcritical flow conditions. In contrast, Figure 4 shows that slopes were steeper and more variable in smaller streams, ranging from 0.75 to 8.83%: the upper end of this range would only be observed in the steepest mountain streams in terrestrial systems, and borders on the slope of debris flows. These very high slopes are found near the edge of the ice sheet near the glacial terminus (the final point of DS534 lower was only 33 m from a terminal moraine), in a similar terminal environment to where Knighton (1981) observed slopes of up to 25% in a temperate Norwegian glacier. These steep slopes led to supercritical flow regimes in 22 of 41 observation sites where slope was measured, with Fr ranging from 0.45 to 3.11. These observations of supercritical flows are consistent with previous studies (Ferguson, 1973; Parker, 1975; Knighton, 1981, 1985; Marston, 1983), with Fr sometimes exceeding those found in terrestrial rivers (Fr ranges from 0.07 to 2.5 as summarized by Wu and Wang, 1999). However, these Fr are largely consistent with those previously reported for supraglacial streams, as Marston (1983) found Fr to range from 0.57 to 2.14.

Our calculations for Manning's *n* are surprising, as they are higher and more variable than might be expected for channels with no sediment or bedforms comprised of sediment and simple rectangular cross-section: *n* ranged from 0.012 to 0.154 with

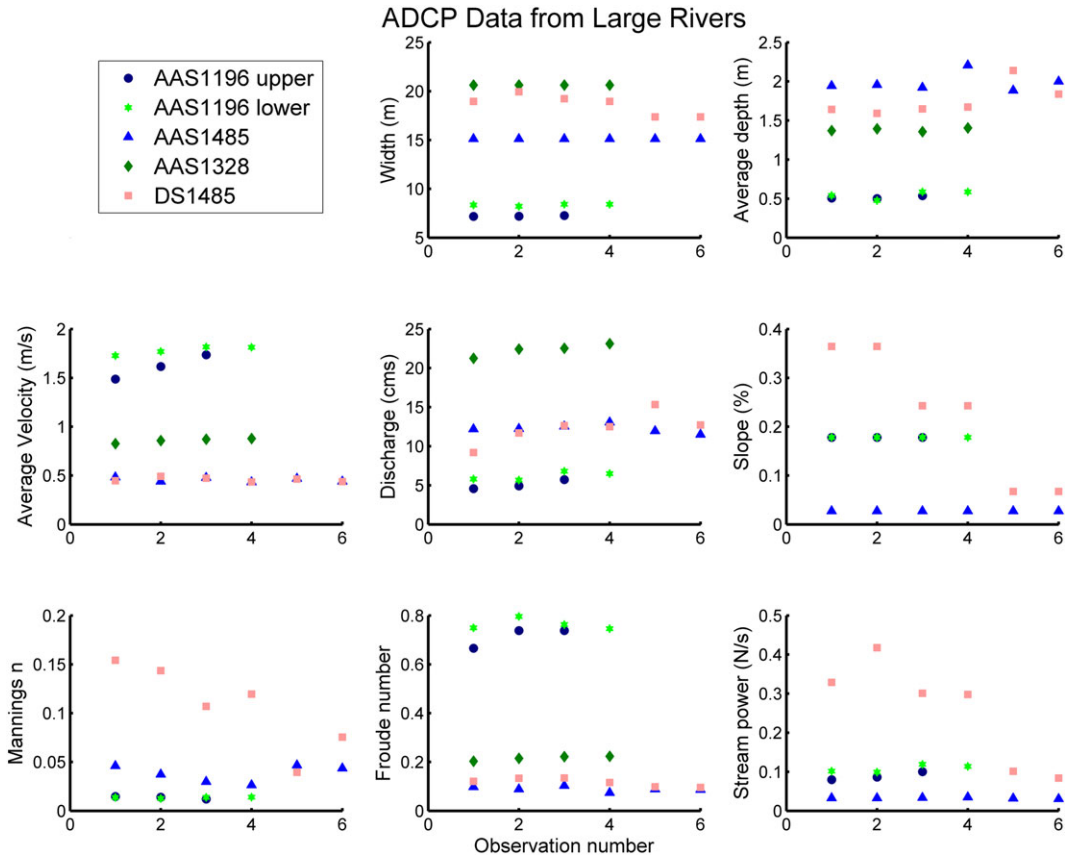

Figure 3. Five *in situ* datasets were obtained for four large channels (7.19–20.62 m wide) via ADCP at elevations from 1196 to 1485 m. At-a-station datasets (rivers beginning with 'AAS') were collected over a period of less than two hours, while dataset DS1485 was made by moving the ADCP in a downstream direction to six different cross-sections (Figure 1) over a period of less than one hour. Note that this means that the *x* axis corresponds to time for the AAS rivers and space for the DS1485. These streams are quite large, and have a maximum discharge of 23.12 m^3/s, two orders of magnitude larger than any previously recorded *in situ* supraglacial discharge. Streams were rougher than expected and Manning's *n* was also quite variable, suggesting that assuming a constant roughness for channels of this scale is inappropriate. Note that discharge, slope, Manning's *n*, Froude number, and stream power are derived from width, depth, and velocity measurements. This figure is available in colour online at wileyonlinelibrary.com/journal/esp

Copyright © 2016 John Wiley & Sons, Ltd.

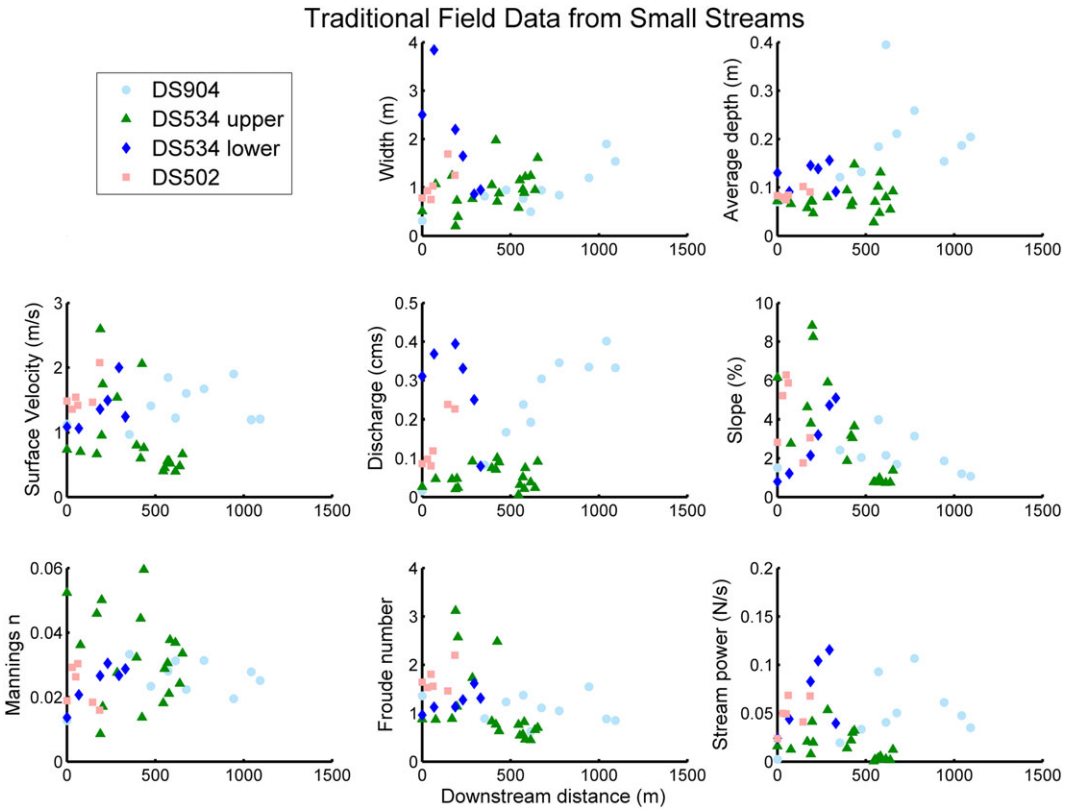

Figure 4. Four *in situ* datasets were obtained for three small channels (0.20–3.84 m wide) via traditional field methods. These datasets reveal streams that are hydraulically heterogeneous and exceed hydraulic expectations for terrestrial streams of a similar scale. Froude number (Fr) was much larger than in terrestrial streams and supercritical flow was common, but Fr largely agreed with previous measurements of supraglacial streams. Streams also had very steep slopes, and these steep slopes occurred on sinuous/meandering planforms that would only be found on gentler slopes in terrestrial environments. As with the larger rivers sampled by ADCP, Manning's *n* was both larger and more variable than expected for these streams of uniform ice substrate. Note that discharge, slope, Manning's *n*, Froude number, and stream power are derived from width, depth, and velocity measurements. This figure is available in colour online at wileyonlinelibrary.com/journal/esp

Table III. Ranges and central tendency (mean, coefficient of variation [CV]) of hydraulic parameters across scales for this study

	Minimum	Maximum	Mean	CV	Number of observations	Unit
Rivers						
w	7.19	20.62	14.79	0.34	23	m
d	0.48	2.89	1.38	0.45	23	m
$\overline{v}$	0.43	1.82	0.91	0.62	23	m/s
Q	*4.58*	*23.12*	*12.04*	*0.48*	*23*	m^3/s
S	*0.027*	*0.364*	*0.145*	*0.76*	*23*	%
Fr	*0.074*	*0.796*	*0.317*	*0.92*	*23*	–
n	*0.012*	*0.154*	*0.051*	*0.92*	*23*	–
Ω	*0.03*	*0.42*	*0.13*	*0.92*	*23*	N/s
Streams						
w	0.20	3.84	1.13	0.58	41	m
d	0.03	0.40	0.11	0.60	41	m
v_{surf}	0.40	2.60	1.19	0.46	41	m/s
Q	*0.006*	*0.402*	*0.146*	*0.86*	*41*	m^3/s
S	*0.737*	*8.827*	*2.776*	*0.76*	*41*	%
Fr	*0.446*	*3.116*	*1.205*	*0.50*	*41*	–
n	*0.009*	*0.060*	*0.029*	*0.39*	*41*	–
Ω	*0.000*	*0.116*	*0.034*	*0.94*	*41*	N/s

Note: Derived quantities are shown in italic typeface.

a coefficient of variation of 0.92 for the larger rivers in this study (Table III). The maximum value of 0.154 is very rough, akin to floodplain flow in medium to dense brush or very weedy channel flow (Chow, 1959). However, only one dataset (DS1485) had *n* values this high: a maximum *n* of 0.047 was observed across all other large river reaches. For the smaller scale streams in our study, *n* ranged from 0.009 to 0.060 with a coefficient of variation of 0.39, which is similar to four out of five of our larger scale rivers and Marston's (1983) reported *n* range of 0.013 to 0.039 in supraglacial channels. Manning's *n* values at the lower end of this range indicate very smooth channels and are akin to straight terrestrial channels with few obstructions, but an *n* of 0.060 is still quite rough and would indicate winding channels with stones, weeds, and pools in terrestrial systems (Chow, 1959). This result also mirrors Marston's (1983) findings and his conclusion that *n* varies more widely than might be expected. Table III summarizes the ranges and central tendency for each of our derived variables at each scale.

Channels were deeply incised at both scales, so, AHG *b* was correspondingly low (maximum of 0.05) for our at-a-station data (all of which were collected at the larger scale via ADCP, Table IV). This agrees with Marston's (1983) AHG results for three streams on a temperate Alaskan glacier with discharges ranging from 0.04 to 0.20 m^3/s, two orders of magnitude less than our at-a-station data. It is important to note that our at-a-station data contain at most six observations taken within a two hour time span, and while there were noticeable changes in discharge during the observational period (Figure 3), our AHG data is far less complete than Marston's, who collected hourly measurements for six days. Thus, our AHG regressions are statistically weak, yet AHG *b* exponents do conform to our expectations given the rectangular cross-sectional geometry of the channels. AHG *f* and *m* values are unusual and range from −0.08 to 0.30 and 0.63 to 0.95, respectively.

The DHG of streams in our study is similar to DHG in terrestrial streams and to DHG previously reported for supraglacial streams (Table IV). In terrestrial systems, review of numerous studies

Copyright © 2016 John Wiley & Sons, Ltd.

Table IV. Table of at-a-station hydraulic geometry (AHG) and downstream hydraulic geometry (DHG) values for this and previous supraglacial studies

	a	*b*	*c*	*f*	*k*	*m*
DHG						
DS904	0.38	0.49	−0.57	0.32	0.15	0.08
DS534 upper	0.42	0.35	−0.59	0.40	0.12	0.17
DS534 lower	0.63	0.65	−0.80	0.19	0.12	0.00
DS502	0.55	0.60	−0.88	0.20	0.34	0.17
Knighton (1981)	0.91	0.26	0.17	0.29	6.46	0.45
Knighton (1981)	1.08	0.30	0.41	0.52	2.02	0.13
Knighton (1981)	1.19	0.30	0.21	0.32	4.02	0.38
AHG						
AAS1328	1.31	0.00	−0.06	0.15	−1.12	0.84
AAS1196 upper	0.81	0.05	−0.50	0.30	−0.24	0.63
AAS1485	1.17	0.00	0.38	−0.08	−1.38	0.95
Marston (1983)	n/a	0.11	n/a	0.34	n/a	0.37
Marston (1983)	n/a	0.10	n/a	0.54	n/a	0.58
Marston (1983)	n/a	0.08	n/a	0.43	n/a	0.46

Note: Parameters *a*, *b*, *c*, *f*, *k*, and *m* are derived in Equations 4, 5, and 6 and explained in Table II.

indicates DHG predictably tends toward $b \approx 0.5$, and $f \approx m \approx 0.2$–0.3 (Gleason, 2015). Our results agree with these previously published values, as DHG *b* values (the rate at which width changes with discharge, Equation 4) in this study ranged from 0.35 to 0.60 and *f* and *m* values (Equations 5 and 6) ranged from 0.17 to 0.40 (excluding DS534 lower). This is in contrast to Knighton (1981), who found DHG *m* values higher than expected at the expense of *b* in two small supraglacial streams in Norway with discharge an order of magnitude less than our smaller scale rivers.

Results of sensitivity analysis on velocity dependent hydraulics

Our two scales of observation involved using two different methods for measuring velocity: surface velocity in the case of streams and depth averaged velocity in the case of rivers. We evaluated the potential bias introduced by velocity measurement technique to velocity dependent hydraulics in Equations 1–6 according to Equation 10, as developed earlier. In the cases of *Q* and Fr, this bias propagates linearly, such that a 15% change in *v* (from Equation 10) produces a 15% change in *Q* and Fr. Assuming such a bias for the smaller streams would reduce our exceptionally high maximum Fr of 3.11 to 2.64, closer to Wu and Wang's (1999) maximum of 2.5 and Marston's (1983) maximum of 2.14. For larger rivers, all Fr would remain below one even with a 15% increase from average to surface velocity, consistent with the low slopes of these streams. The resultant changes in *Q* would affect DHG coefficients, but not DHG exponents (the latter are generally considered of greater fluvial interest and are scale independent), and likewise AHG exponents are a function of channel geometry and remain unchanged (Gleason, 2015).

Computing average velocity in smaller streams allows direct comparison between Manning's *n* across scales, as the ADCP was able to directly measure average velocity for the larger rivers. The updated small-stream *n* range becomes 0.007–0.051, consistent with the range 0.014–0.047 found in larger rivers (excluding DS1485). Conversely, if we use surface velocity to calculate *n* at both scales, *n* ranges 0.008–0.059 and 0.016–0.055 in smaller and larger channels, respectively, yielding *n* values that are consistent across scales but also highly variable. In sum, while we would have ideally been able to measure vertical velocity profiles in all channels, our smaller streams were simply too shallow for our equipment to do so. However, using measured surface velocity did not substantially impact the interpretation and main implications of our results, despite having a non-trivial influence on the actual values of the hydraulic quantities we calculated. Thus, the following discussion and interpretation of our results refers to hydraulic quantities derived from the original *in situ* velocity measurements (surface in small streams, depth-averaged in larger channels) in each case.

Discussion

Our results indicate that Greenland's supraglacial streams and rivers are heterogeneous: observed and derived hydraulic parameters were highly variable in channels at both scales, yet the degree of variability was similar for most parameters. For example, channels of both scales had considerable overlap in *n*, but *n* ranges are quite large and do not exhibit strong central tendency at either scale, and slope and Fr were similarly variable across scales (Table III). Reaches at both scales did have similar deeply incised channel geometry and similar ice substrate, yet despite this similarity and despite having broadly similar hydraulic ranges, channels of different scales were distinct from one another: larger rivers in this study were smoother, deeper, and had lower width/depth ratios than smaller scale streams. While these differences reflect a sampling bias toward gentle sloping large channels for safety reasons, these results highlight the large hydraulic variability in our channels, and suggest that assuming constant values for hydraulic parameters (particularly *n* and Fr) is inappropriate.

Manning's *n* and flow resistance in supraglacial channels

Our largest *n* values, found at both scales, are akin to those found in vegetated channels with irregular sides (Chow,

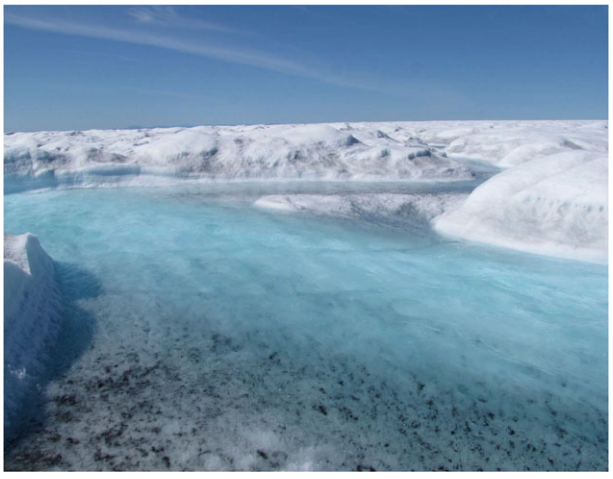

Figure 5. This photograph is typical of channels in this study, and shows cryoconite pitting (foreground), channel wall scalloping (lower left), and ice cracks that persist to the channel bed (running transverse across the center of the image). This figure illustrates the ubiquitous presence of cryoconite in the shallower and slower flow in the foreground and background and the relatively clean channel bed in the thalweg. Because cryoconite is associated with local pitting, this should yield asymmetric roughness across the channel and could help explain the elevated roughness of our channels, yet we speculate that other factors besides bed roughness contribute to the high flow resistance observed here. This figure is available in colour online at wileyonlinelibrary.com/journal/esp

Copyright © 2016 John Wiley & Sons, Ltd.

1959). These high *n* were observed despite no flow impediments in the channels and little to no suspended sediment. In terrestrial systems, *n* is primarily a function of bed roughness elements and channel form, and following this paradigm in our channels leads to several hypotheses as to why these uniform substrate channels exhibited such high *n* values. First, ice stresses produce longitudinal cracks that intersect channels and persist in the bed, creating channel irregularities. These cracks, along with the scalloping effect described by Marston (1983), likely contributed to the increased roughness observed across scales (see the channel wall, lower left, and transverse channel cracks in Figure 5). Our observations also indicate that cryoconite pitting may be an additional and overlooked contributor to bed roughness in certain sections of streams where cryoconite is prevalent (Figure 5). Cryoconite was absent in the thalweg of smaller streams, and completely absent in the large rivers at high elevations, despite the widespread distribution of cryoconite holes adjacent to the channels in each case. Thus, our observations also suggest that any cryoconite-induced contributions to *n* may vary in a cross-stream direction as the channel transitions to faster and deeper flow and where cross-stream cryoconite pitting is not evenly distributed in the channel.

Despite these plausible mechanisms for increased bed roughness, they are unlikely to yield such high *n* values on their own. This is because Manning's *n*, while commonly interpreted as a function of bed roughness in terrestrial systems (and rightly so), is in fact a manifestation of the wider physical principle of flow resistance. Thus, our elevated and widely ranging *n* values suggest channels offering significant resistance to flow. We speculate that the lower observed *n* values, which suggest smooth artificial channels, are indeed a consequence of minimal bed roughness, but that larger *n* values are associated with other sources of flow resistance. One plausible source of this resistance is the presence of suspended slush ice in channels, especially at lower flows, as we visually observed slush in numerous cases but did not quantify its presence. Additionally, crack-induced turbulence can manifest as flow resistance if water enters into cracks at significant depths. The low temperature of the water in these channels would increase the fluid viscosity and thus also could have affected the velocity profile. Future work should explicitly consider these and other forms of flow resistance, which will require field observations of more than just the basic quantities measured here. Further research also might use hydraulic models to examine these concepts and provide a more process-based understanding of these

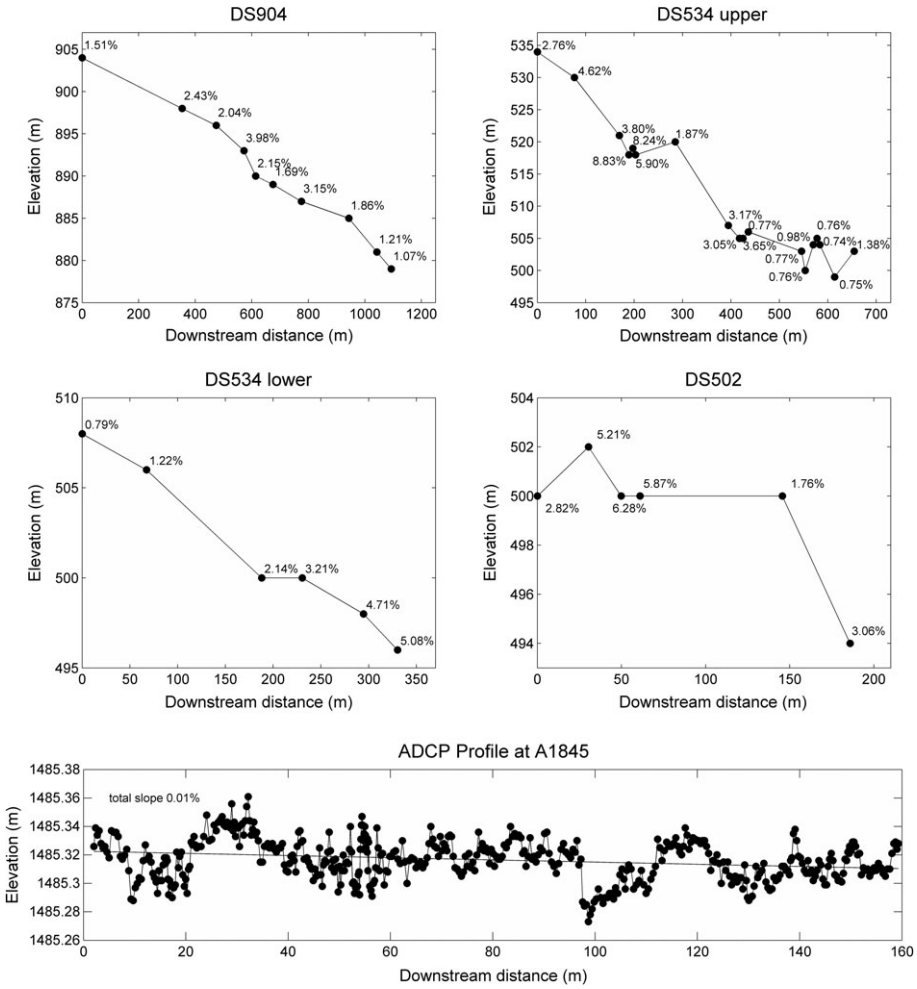

Figure 6. Downstream elevation profiles collected with eTrex global positioning system (GPS) measurements (with autolevel-derived local water surface slope labeled at each measurement site) of *in situ* water surface slopes (expressed as a percent change in height/reach length) sampled along four streams in the same watershed are shown here (one imprecise GPS elevation measurement from DS534 upper was removed to make this plot). The slope of DS904 (at 904 m elevation) is lower than the three other datasets collected 400 m lower in elevation, suggesting an ice surface that increases in steepness as it loses elevation: consistent with glaciological understanding of the Greenland Ice Sheet (GrIS). This is in contrast to terrestrial expectations of a watershed, where steeper slopes typically are found at higher elevations. Additionally, water surface slopes for DS534 lower mirror this trend, as this channel steepens as it moves downstream. The ADCP profile collected below the site at AAS1485 shows that the larger rivers in this study had much lower slopes than the smaller streams, with a total slope of 0.01% over 160 m.

Copyright © 2016 John Wiley & Sons, Ltd.

observations. Modeling efforts also should consider the effects of cryoconite on both stream development (as the strong thermal controls on streams will be affected by increased cryoconite albedo) and stream hydraulics.

Slope and Froude number in supraglacial channels

In addition to elevated flow resistance, our smaller-scale field data were inconsistent with theories describing the hydraulics of such steep channels found on land. In contrast to expectations based on terrestrial watersheds where steeper streams are found in the headwaters at higher elevations, Figure 6 shows the water surface slopes of DS534 and DS502 were higher than those of DS904, located 400 m above these lower streams in the same watershed. This is consistent with glaciological characterization of the GrIS, where ablation, crevassing and other stresses increase at the ice margin, thus increasing local surface slope. Similarly, water surface slope actually increased with decreasing elevation for DS534 lower, suggesting a channel that steepens in the downstream direction (Figure 6). In addition, terrestrial streams with slopes greater than 5% would be expected to be either braided or full of boulders and other debris (Rosgen, 1994), but supraglacial streams here lacked the sediment required for either of these phenomena to develop. Thus, the unique supraglacial environment allows for planforms typically found on gentle slopes in terrestrial settings to occur on steep sections in this supraglacial environment.

These steep slopes in turn yielded higher Fr than typical in terrestrial streams, with supercritical flow observed in 54% of our measurement sites in smaller streams. While consistent with previous research, our reported range of Fr (up to 3.11) is higher than Fr previously found in supraglacial systems, yet the sensitivity analysis reported earlier shows that using average velocity instead of measured surface velocity reduces this maximum to agree with previously published values. These high Fr were only found in smaller streams at lower elevation, and were consistent with the very high AHG *m* values found there. Our results affirm that supercritical flow is common in smaller supraglacial streams and that hydraulic models applied to supraglacial streams must be capable of representing both subcritical and supercritical flow regimes in such environments.

Hydraulic geometry of supraglacial channels

Ferguson's (1986) derivation of AHG revealed that AHG exponents are controlled entirely by cross-sectional geometry, provided a few key assumptions about flow depth and bed roughness are valid. Given his conclusions, our AHG exponent values would suggest deeply incised channels with near vertical walls, exactly as we observed. Additionally, the similar AHG results between our study and Marston's (1983) covering two orders of magnitude in discharge, suggest that Ferguson's key assumption that flows are relatively deep with $R/D_{90} > 10^2$ (where D_{90} is the 90th percentile of the bed material grain size distribution) holds across scales and may be applied more generally to the ice sheet, despite a lack of a clear analog for bed grain size in this ice environment. Our study and Marston's (1983) both found very high AHG *m* values, suggesting that as discharge in supraglacial rivers increases in response to the strong diurnal forcing of insolation, flow velocities increase at a greater rate than depths at-a-station (Table IV). In contrast to AHG, the DHG of our supraglacial channels was similar to the DHG expected in terrestrial rivers: widths, depths, and velocities increased in a downstream direction at similar rates to streams found on land. This similarity is observed despite the ubiquitous addition of flow to channels due to melting of channel walls and other lateral inflow in the thermally-driven supraglacial environment.

Conclusions

Our investigation of supraglacial channels on the GrIS revealed that these features are sometimes quite dissimilar from terrestrial systems and hydraulically heterogeneous. While all investigated channels were deeply incised, Manning's *n*, Fr numbers, water surface slope, and stream power all exhibited a wide range of values across our nine study reaches. Compared to the smaller field studies of Marston and Knighton conducted in the 1980s, our results have revealed numerous similarities between streams of the GrIS and smaller marginal streams on alpine glaciers. These hydraulic similarities occur despite presence of debris in those alpine streams and despite the two orders of magnitude increase in scale in our Greenland sites. While this similarity across scales is encouraging, the most important similarity across these studies is the heterogeneity of hydraulics, as supraglacial channels are found to have diverse roughness, velocity, and slopes within and across all scales. Therefore, our results suggest that the intuitive assumption following from classic hydraulics that uniform ice substrate should lead to uniform hydraulic behavior in supraglacial channels is not valid.

Future work should seek to assess whether the wide ranges of parameters reported here (and previously) represent end members of a distribution of hydraulic quantities, examine any physical limits to these hydraulics in the unique supraglacial environment, and assess whether geomorphic discriminants may be used to usefully categorize supraglacial channels, much like Rosgen (1994) proposed for terrestrial streams. Given the important differences between supraglacial and terrestrial systems chronicled here, future research attempting to model or characterize supraglacial streams should consider the influence of cryoconite on both thermal erosion and flow resistance, allow for a wide range of hydraulic variable values (particularly *n* and Fr), and take care when applying terrestrial hydraulic theory without field-based verification. Moreover, this work has revealed the urgent need for more detailed *in situ* research of the supraglacial environment, especially investigation of flow resistance. While this work is logistically challenging, such an effort is necessary to inform the increasing literature that leverages satellite imagery and DEMs to understand the hydrologic and hydraulic behavior of the ice surface and ultimately the role of supraglacial channels in providing runoff to the global ocean.

Acknowledgements—This research was supported by the NASA Cryosphere Program (grant NNX11AQ38G) managed by Dr. Thomas Wagner. CH2MHill and Kangerlussuaq International Science Support (KISS) provided logistical support, and the authors would like to thank Kathy Young, Susan Zager, and Tonny Olsson for their help in making difficult fieldwork as easy as possible. J. Toby Minear provided useful comments on an earlier version of this document, and the authors thank him and Irina Overeem and one anonymous reviewer for their suggestions that have improved this paper. Any use of trade, firm, or product names is for descriptive purposes only and does not imply endorsement by the US Government.

References

Andersen ML, Stenseng L, Skourup H, Colgan W, Khan SA, Kristensen SS, Andersen SB, Box JE, Ahlstrøm AP, Fettweis X, Forsberg R. 2015. Basin-scale partitioning of Greenland ice sheet mass balance

Copyright © 2016 John Wiley & Sons, Ltd.

components (2007–2011). *Earth and Planetary Science Letters* **409**: 89–95. DOI:10.1016/j.epsl.2014.10.015.

Barletta VR, Sørensen LS, Forsberg R. 2013. Scatter of mass changes estimates at basin scale for Greenland and Antarctica. *The Cryosphere* **7**: 1411–1432. DOI:10.5194/tc-7-1411-2013.

Bøggild CE, Brandt RE, Brown KJ, Warren SG. 2010. The ablation zone in northeast Greenland: ice types, albedos and impurities. *Journal of Glaciology* **56**: 101–113. DOI:10.3189/002214310791190776.

Chow VT. 1959. Open-channel Hydraulics. Reprinted 2009. The Blackburn Press: Caldwell, NJ.

Chu VW. 2014. Greenland ice sheet hydrology: a review. *Progress in Physical Geography* **38**(1): 19–54. DOI:10.1177/0309133313507075.

Enderlin EM. 2014. An improved mass budget for the Greenland ice sheet. *Geophysical Research Letters* **41**(3): 866–872. DOI:10.1002/2013GL059010.R.

Ferguson RI. 1973. Sinuosity of supraglacial streams. *Geological Society of America Bulletin* **84**: 251–256. DOI:10.1130/0016-7606(1973)84<251:SOSS>2.0.CO;2.

Ferguson RI. 1986. Hydraulics and hydraulic geometry. *Progress in Physical Geography* **10**: 1–31. DOI:10.1177/030913338601000101.

Fitzpatrick AAW, Hubbard AL, Box JE, Quincey DJ, van As D, Mikkelsen APB, Doyle SH, Dow CF, Hasholt B, Jones GA. 2014. A decade (2002–2012) of supraglacial lake volume estimates across Russell Glacier, west Greenland. *The Cryosphere* **8**: 107–121. DOI:10.5194/tc-8-107-2014.

Gleason CJ. 2015. Hydraulic geometry of natural rivers: a review and future directions. *Progress in Physical Geography* **39**(3): 337–360. DOI:10.1177/0309133314567584.

Hall DK, Comiso JC, DiGirolamo NE, Shuman CA, Box JE, Koenig LS. 2013. Variability in the surface temperature and melt extent of the Greenland ice sheet from MODIS. *Geophysical Research Letters* **40**: 2114–2120. DOI:10.1002/grl.50240.

Hasholt B, Bech Mikkelsen A, Holtegaard Nielsen M, Andreas Dahl Larsen M. 2013. Observations of runoff and sediment and dissolved loads from the Greenland Ice Sheet at Kangerlussuaq, west Greenland, 2007 to 2010. *Zeitschrift für Geomorphologie Supplementary Issues* **57**: 3–27. DOI:10.1127/0372-8854/2012/S-00121.

Jarosch AH, Gudmundsson MT. 2012. A numerical model for meltwater channel evolution in glaciers. *The Cryosphere* **6**: 493–503. DOI:10.5194/tc-6-493-2012.

Joughin I, Das SB, Flowers GE, Behn MD, Alley RB, King MA, Smith BE, Bamber JL, van den Broeke MR, van Angelen JH. 2013. Influence of ice-sheet geometry and supraglacial lakes on seasonal ice-flow variability. *The Cryosphere* **7**: 1185–1192. DOI:10.5194/tc-7-1185-2013.

Karlstrom L, Gajjar P, Manga M. 2013. Meander formation in supraglacial streams. *Journal of Geophysical Research - Earth Surface* **118**: 1897–1907. DOI:10.1002/jgrf.20135.

Karlstrom L, Yang K. 2016. Fluvial supraglacial landscape evolution on the Greenland Ice Sheet. *Geophysical Research Letters* **43**: 2683–2692. DOI:10.1002/2016GL067697.

Kingslake J, Sole A. 2015. Modelling channelized surface drainage of supraglacial lakes. *Journal of Glaciology* **61**: 185–199. DOI:10.3189/2015JoG14J158.

Knighton AD. 1972. Meandering habit of supraglacial streams. *Geological Society of America Bulletin* **83**: 201–204. DOI:10.1130/0016-7606(1972)83[201:MHOSS]2.0.CO;2.

Knighton AD. 1981. Channel form and flow characteristics of supraglacial streams, Austre Okstindbreen, Norway. *Arctic and Alpine Research* **13**: 295–306. DOI:10.2307/1551036.

Knighton AD. 1985. Channel form adjustment in supraglacial streams, Austre Okstindbreen, Norway. *Arctic and Alpine Research* **17**: 451–466. DOI:10.2307/1550870.

Lampkin DJ, VanderBerg J. 2014. Supraglacial melt channel networks in the Jakobshavn Isbræ region during the 2007 melt season. *Hydrological Processes* **28**: 6038–6053. DOI:10.1002/hyp.10085.

Leopold LB, Maddock Jr T. 1953. The Hydraulic Geometry of Stream Channels and Some Physiographic Implications, US Geological Survey Professional Paper 252. US Geological Survey: Reston, VA.

Legleiter CJ, Tedesco M, Smith LC, Behar AE, Overstreet BT. 2014. Mapping the bathymetry of supraglacial lakes and streams on the Greenland Ice Sheet using field measurements and high-resolution satellite images. *The Cryosphere* **8**: 215–228. DOI:10.5194/tc-8-215-2014.

Lindbäck K, Pettersson R, Hubbard AL, Doyle SH, van As D, Mikkelsen AB, Fitzpatrick AA. 2015. Subglacial water drainage, storage, and piracy beneath the Greenland Ice Sheet. *Geophysical Research Letters* **42**(18): 7606–7614. DOI:10.1002/2015GL065393.

MacDonell S, Fitzsimons S. 2008. The formation and hydrological significance of cryoconite holes. *Progress in Physical Geography* **32**: 595–610. DOI:10.1177/0309133308101382.

Marston RA. 1983. Supraglacial stream dynamics on the Juneau Icefield. *Annals of the Association of American Geographers* **73**: 597–608. DOI:10.1111/j.1467-8306.1983.tb01861.x.

McGrath D, Colgan W, Steffen K, Lauffenburger P, Balog J. 2011. Assessing the summer water budget of a moulin basin in the Sermeq Avannarleq ablation region, Greenland Ice Sheet. *Journal of Glaciology* **57**: 954–964. DOI:10.3189/002214311798043735.

Mernild SH, Hasholt B. 2009. Observed runoff, jökulhlaups and suspended sediment load from the Greenland ice sheet at Kangerlussuaq, west Greenland, 2007 and 2008. *Journal of Glaciology* **55**: 855–858. DOI:10.3189/002214309790152465.

Mikkelsen AB, Hasholt B, Knudsen NT, Nielsen MH. 2013. Jökulhlaups and sediment transport in Watson River, Kangerlussuaq, west Greenland. *Hydrology Research* **44**: 58. DOI:10.2166/nh.2012.165.

Mueller DS. 2013. Extrap: Software to assist the selection of extrapolation methods for moving-boat ADCP streamflow measurements. *Computers & Geosciences* **54**: 211–218. DOI:10.1016/j.cageo.2013.02.001.

Nobles LH. 1960. Glaciological Investigations, Nunatarssuaq Ice Ramp, Northwestern Greenland, US Army Cold Regions Research & Engineering Laboratory, Technical Report 66. Engineering Research and Development Center: Vicksburg, MS; 57 p.

Overeem I, Hudson B, Welty E, Mikkelsen A, Bamber J, Petersen D, Lewinter A, Hasholt B. 2015. River inundation suggests ice-sheet runoff retention. *Journal of Glaciology* **61**: 776–788. DOI:10.3189/2015JoG15J012.

Parker G. 1975. Meandering of supraglacial melt streams. *Water Resources Research* **11**: 551–552. DOI:10.1029/WR011i004p00551.

Poinar K, Joughin I, Das SB, Behn MD, Lenaerts JTM, van den Broeke MR. 2015. Limits to future expansion of surface-melt-enhanced ice flow into the interior of western Greenland. *Geophysical Research Letters* **42**(6): 1800–1807. DOI:10.1002/2015GL063192.

Rantz SE *et al.* 1982. Measurement and Computation of Streamflow, Volumes 1 and 2, USGS Water Supply Paper 2175. US Geological Survey: Reston, VA.

Rennermalm AK, Moustafa SE, Mioduszewski J, Chu VW, Forster RR, Hagedorn B, Harper JT, Mote TL, Robinson DA, Shuman CA, Smith LC, Tedesco M. 2013a. Understanding Greenland Ice Sheet hydrology using an integrated multi-scale approach. *Environmental Research Letters* **8**: 015017. DOI:10.1088/1748-9326/8/1/015017.

Rennermalm AK, Smith LC, Chu VW, Box JE, Forster RR, Van den Broeke MR, Van As D, Moustafa SE. 2013b. Evidence of meltwater retention within the Greenland Ice Sheet. *The Cryosphere* **7**: 1433–1445. DOI:10.5194/tc-7-1433-2013.

Rignot E, Box JE, Burgess E, Hanna E. 2008. Mass balance of the Greenland Ice Sheet from 1958 to 2007. *Geophysical Research Letters* **35**: L20502. DOI:10.1029/2008GL035417.

Robert A. 2003. River Processes: An Introduction to Fluvial Dynamics. Arnold: London; 214 pp.

Rosgen DL. 1994. A classification of natural rivers. *Catena* **22**(3): 169–199. DOI:10.1016/0341-8162(94)90001-9.

Sasgen I, van den Broeke M, Bamber JL, Rignot E, Sørensen LS, Wouters B, Martinec Z, Velicogna I, Simonsen SB. 2012. Timing and origin of recent regional ice-mass loss in Greenland. *Earth and Planetary Science Letters* **333–334**: 293–303. DOI:10.1016/j.epsl.2012.03.033.

Schrama E, Wouters B, Vermeersen B. 2011. Present day regional mass loss of Greenland observed with satellite gravimetry. *Surveys in Geophysics* **32**: 377–385. DOI:10.1007/s10712-011-9113-7.

Smith LC, Chu VW, Yang K, Gleason CJ, Pitcher L H, Rennermalm AK, Legleiter CJ, Behar AE, Overstreet BT, Moustafa SE, Tedesco M, Forster RR, LeWinter AL, Finnegan DC, Sheng Y, Balog J. 2015. Efficient meltwater drainage through supraglacial streams and rivers on the southwest Greenland Ice Sheet. *Proceedings of the National Academy of Sciences* **112**: 1001–1006. DOI:10.1073/pnas.1413024112.

Copyright © 2016 John Wiley & Sons, Ltd.

Tedesco M, Foreman CM, Anton J, Steiner N, Schwartzman T. 2013. Comparative analysis of morphological, mineralogical and spectral properties of cryoconite in Jakobshavn Isbrae, Greenland, and Canada Glacier, Antarctica. *Annals of Glaciology* **54**: 147–157. DOI:10.3189/2013AoG63A417.

van den Broeke M, Bamber J, Ettema J, Rignot E, Schrama E, van de Berg WJ, van Meijgaard E, Velicogna I, Wouters B. 2009. Partitioning recent Greenland mass loss. *Science* **326**: 984–986. DOI:10.1126/science.1178176.

Wientjes IGM, Van de Wal RSW, Reichart GJ, Sluijs A, Oerlemans J. 2011. Dust from the dark region in the western ablation zone of the Greenland Ice Sheet. *The Cryosphere* **5**: 589–601. DOI:10.5194/tc-5-589-2011.

Wu W, Wang SSY. 1999. Movable bed roughness in alluvial rivers. *Journal of Hydraulic Engineering* **125**: 1309–1312. DOI:10.1061/(ASCE)0733-9429(1999)125:12(1309).

Yang K, Smith LC. 2013. Supraglacial streams on the Greenland Ice Sheet delineated from combined spectral shape information in high-resolution satellite imagery. *IEEE Geoscience and Remote Sensing Letters* **10**: 801–805. DOI:10.1109/LGRS.2012.2224316.

Yang K, Smith LC, Chu VW, Gleason CJ, Li M. 2015. A caution on the use of surface digital elevation models to simulate supraglacial hydrology of the Greenland Ice Sheet. *IEEE Journal of Selected Topics in Applied Earth Observations and Remote Sensing*. DOI:10.1109/JSTARS.2015.2483483.

Yang K, Smith LC, Chu VW, Pitcher LH, Gleason CJ, Rennermalm AK, Li M. 2016. Fluvial morphometry of supraglacial river networks on the southwest Greenland Ice Sheet. *GIScience & Remote Sensing*. DOI:10.1080/15481603.2016.1162345.

Zwally HJ, Jun L, Brenner AC, Beckley M, Cornejo HG, Dimarzio J, Giovinetto MB, Neumann TA, Robbins J, Saba JL, Donghui Y, Wang W. 2011. Greenland ice sheet mass balance: distribution of increased mass loss with climate warming; 2003–07 versus 1992–2002. *Journal of Glaciology* **57**: 88–102. DOI:10.3189/002214311795306682.

Zwally HJ, Giovinetto MB, Li J, Cornejo HG, Beckley MA, Brenner AC, Saba JL, Yi D. 2005. Mass changes of the Greenland and Antarctic ice sheets and shelves and contributions to sea-level rise: 1992–2002. *Journal of Glaciology* **51**: 509–527. DOI:10.3189/172756505781829007.

Copyright © 2016 John Wiley & Sons, Ltd.